Channel-Based ICXT- and NLI-Aware Service Provisioning for Multi-Band over SDM Systems

Arash Rezaee[1], Farhad Arpanaei[2], Ryan McCann[1], Hami Rabbani[3],
José Alberto Hernández[2], Maite Brandt-Pearce,[3] and Vinod M. Vokkarane[1,*]
[1]*Electrical and Computer Engineering Department, University of Massachusetts Lowell, United States,*
[2]*Department of Telematic Engineering, Universidad Carlos III de Madrid, 28911, Leganes, Madrid, Spain,*
[3]*Charles L. Brown Department of Electrical and Computer Engineering, University of Virginia, United States,*
[*]Vinod_Vokkarane@uml.edu

***Abstract*—The relentless surge in bandwidth demands fueled by 5G and beyond necessitates a paradigm shift in optical network design. This paper introduces a novel, channel-based resource allocation framework for multi-band over space-division multiplexing optical networks, meticulously addressing the intertwined challenges of inter-core crosstalk (ICXT), inter-channel stimulated Raman scattering (ISRS), and fiber non-linear impairments. By leveraging a sophisticated generalized signal-to-noise ratio model that dynamically accounts for frequency-dependent ICXT and ISRS, we propose two innovative algorithms—Core-Spectrum-Band (CSB) and Band-Spectrum-Core (BSC)—to optimize resource allocation for multi-core fiber (MCF) and compare their performance with bundled multi-fiber pair (BuMFP) architectures. Extensive simulations on the US Backbone network demonstrate the superior performance of our approach, significantly reducing blocking probability. Specifically, in a network with seven cores/fibers, BSC with MCF reduced the blocking probability by approximately 70% and 20% compared to BuMFPs and CSB with MCF, respectively, on average across traffic loads ranging from 1000 to 1450 Tbps.**

I. Introduction

With the rise of 5G and beyond, along with the rapid expansion of Internet of Things devices and high-quality video streaming applications, communication service providers are encountering a substantial surge in demand for high-speed, low-latency services to support bandwidth-intensive applications [1]. Single-core, single-band elastic optical networks (EONs) are insufficient to meet the growing demand, leading to the enhancement of EONs by two resource-expanding approaches: multi-band (MB-EONs) and space-division multiplexing (SDM-EONs) technologies. SDM-EONs employ multi-core fibers (MCFs), few mode fibers (FMF), or FM-MCFs to enhance physical capacity by multiplexing multiple EONs [2], while MB-EONs provide a cost-effective solution to address capacity limitations by utilizing bands beyond the C-band [3]. Integrating MB-EONs over SDM-EONs technology (MBoSDM) and leveraging a bundle of multifiber pairs (BuMFPs) cables offers a substantial increase in network capacity and flexibility, effectively meeting rising bandwidth demands while maximizing the efficiency of physical infrastructure [4], [5].

Inter-core crosstalk (ICXT) is a critical factor in the design and performance of MCFs, as it increases when the distance between adjacent cores is reduced, particularly in fibers using a smaller cladding diameter. Effective ICXT management is essential to enable high-quality, all-optical transmission over long distances without digital signal processing, which depends on factors such as transmission distance, the spacing between adjacent cores, the number of adjacent cores, and the modulation format level [6]. MB-EON systems with inter-channel stimulated Raman scattering (ISRS) introduce additional complexity to the resource management of MBoSDM. Alongside inter-core crosstalk (ICXT), ISRS impacts the quality of transmission and necessitates careful consideration of frequency-dependent power coupling across bands [7], [8]. The mentioned impairments, along with amplified spontaneous emission (ASE) and fiber non-linear impairments (NLIs), pose a significant barrier to the signal-to-noise ratio (SNR) and spectral efficiency of fiber connections, making quality-of-transmission (QoT)-aware resource allocation essential for dynamic optical networks design.

The effects of ICXT and ISRS have been investigated in separate studies, providing a foundation for developing effective resource allocation strategies in optical networks. The effects of link-based and slice-based worst-case ICXT calculation on dynamic lightpath provisioning are investigated in [9]. ICXT-limitation, spectrum utilization, and fragmentation are considered in the resource allocation problem of MCF-EONs to enhance network performance in dynamic lightpath provisioning scenarios [10], [11]. A machine learning-aided lit core threshold optimization strategy is proposed to enhance the performance of arbitrary resource allocation approach by balancing the trade-off between spectrum usage and ICXT effects [12]. ICXT-aware routing, which dynamically adjusts link costs based on the network state, along with ICXT-aware sliceable resource allocation, is presented in [13].

Sambo et al. proposed a resource allocation approach to assess the generalized signal-to-noise ratio (GSNR) across different band combinations, aiming to reduce blocking probability and optimize resource utilization [14]. A spectrum fragmentation- and QoT-aware resource allocation algorithm

The authors from the University of Massachusetts Lowell thank the National Science Foundation (NSF) for supporting this research under award #2008530. The authors from UC3M would like to acknowledge the support of the EU-funded SEASON project (grant No. 101096909), and Spanish funded Fun4date-Redes project (grant No.PID2022-136684OBC21).

978-3-903176-67-6

for MB-EONs is presented in [15], optimizing resource allocation by leveraging fragmentation metrics and QoT to reduce service blocking, with a slight trade-off in path length. A fragmentation- and impairment-aware Q-learning-based routing with a QoT-aware band and spectrum allocation approach for C+L band EONs was proposed in [16]. Also, a heuristic MB-EON resource allocation strategy is proposed in [17] and [18] to realize QoT constraints, which categorizes requests by shortest route length and the longest shortest route in the network, or bit rate, considering the different order of band to each category. Band partition protection scheme for survivable static MBoSDM network design is investigated in [19] dedicating the C-band to working connections and the L-band to protection connections.

This paper introduces two novel approaches, Core-Spectrum-Band (**CSB**) and Band-Spectrum-Core (**BSC**), for resource assignment in MBoSDM networks while considering key impairments. These methods are integrated into a QoT-aware dynamic resource allocation strategy using a software-defined elastic optical network (SD-EON) controller, incorporating a comprehensive analytical GSNR model [20], [21]. A performance study compares MCFs with BuMFPs MB-EONs under varying traffic conditions. Additionally, the introduced approaches and architectures are implemented in the open-source QoT-aware SD-EON controller proposed in [22]. To the best of our knowledge, this is the first work to analyze the dependency of ICXT on channel frequency in the presence of ISRS within the GSNR calculation for dynamic resource allocation.

II. System Model and Physical Layer Modeling

In this work, we consider a multi-layer optical transport network MBoSDM. We use C+L+S-band technology, providing approximately 20 THz of bandwidth. The modulation format of the line card interface (LCI) is adjusted based on a probabilistic constellation-shaping approach. Therefore, the modulation format of each lightpath (LP) depends on the channel and core it utilizes. Therefore, the bit rate of each LCI can be adaptively changed based on the generalized mutual information (GMI), which is a function of the SNR [23].

Additionally, we assume that each link is equipped with cutting-edge technology, specifically, ultra-low-loss and ICXT trench-assisted (TA) MCFs. The ICXT in TA-MCFs depends on fiber parameters such as the relative refractive index difference between the trench and cladding, trench width, and center core-to-core distance. It also depends on the frequency. While the dependency is negligible in C-band optical networks, it becomes significant in multi-band systems such as C+L+S-band technology, which is the system model considered in this work [20]. The analytical frequency-dependent closed-form model for ICXT in TA-MCFs is estimated from (1), inspired by a similar equation proposed in [24].

$$P_{\text{ICXT}}(f^i) \cong \sum_{c' \in \mathcal{N}_{\text{AC}}, c' \neq c} \mu_{\text{ICXT}}(f^i) P_{\text{tx}}(f^i), \tag{1}$$

where, $\mu_{\text{ICXT}}(f^i)$ is calculated from (2).

$$\mu_{\text{ICXT}}(f^i) = \frac{N_{\text{AC}} - N_{\text{AC}} \exp[-(N_{\text{AC}}+1)\Omega(f^i)L]}{1 + N_{\text{AC}} \exp[-(N_{\text{AC}}+1)\Omega(f^i)L]}, \tag{2}$$

and the power coupling coefficient (PCC), is obtained from (3).

$$\Omega(f^i) = \frac{c\kappa^2(f^i) r_{\text{b}} n_{\text{core}}}{\pi f^i \Lambda}, \tag{3}$$

where $\kappa(f^i)$, r_{b}, c, Λ, L, n_{core}, f^i, N_{AC}, and $P_{\text{tx}}(f^i)$ represent the mode coupling coefficient, bending radius, propagation velocity, the distance between the centers of two adjacent cores (or core pitch), transmission distance, effective refractive index of the core, channel's center frequency, the number of lit adjacent cores of the channel under test, and launch power, respectively. Furthermore, the mode coupling coefficient is calculated from equation (3) in [20].

Therefore, the end-to-end QoT of an LP in terms of the GSNR at channel i is estimated from (4) inspired from the incoherent Gaussian noise (GN)/enhanced GN (EGN) model for multi-band systems proposed in [25].

$$GSNR^i_{\text{LP}}|_{\text{dB}} = 10\log_{10}\Big[\big(SNR^{-1}_{\text{ASE}} + SNR^{-1}_{\text{NLI}} + SNR^{-1}_{\text{ICXT}} + SNR^{-1}_{\text{TRx}}\big)^{-1}\Big] - \sigma_{\text{Flt}}|_{\text{dB}} - \sigma_{\text{Ag}}|_{\text{dB}}, \tag{4}$$

where

$$SNR_{\text{ASE}} = \Sigma_{s\in S} P^{s+1,i}_{\text{tx}} / P^{s,i}_{\text{ASE}}, \tag{5}$$

$$SNR_{\text{NLI}} = \Sigma_{s\in S} P^{s+1,i}_{\text{tx}} / P^{s,i}_{\text{NLI}}, \tag{6}$$

$$SNR_{\text{ICXT}} = \Sigma_{s\in S} P^{s+1,i}_{\text{tx}} / P^{s,i}_{\text{ICXT,}} \tag{7}$$

and

$$P^{s,i}_{\text{ASE}} = n_{\text{F}} h f^i (G^{s,i} - 1) R_{\text{ch}}. \tag{8}$$

$P^{s+1,i}_{\text{tx}}$ is the launch power at the beginning of span $s+1$, $P^{s,i}_{\text{ASE}}$ is noise power caused by the doped fiber amplifier (DFA) equipped with the dynamic gain equalizer (DGE), and non-linear interference (NLI) noise power ($P^{s,i}_{\text{NLI}}$) is calculated from (2) in [26]. Moreover, n_{F}, h, f^i, $G^{s,i} = P^{s+1,i}_{\text{tx}}/P^{s,i}_{\text{rx}}$, S, and R_{ch} are the noise figure of DFA, Planck's coefficient, channel frequency, frequency center of the spectrum, the gain of DFA, set of spans, and channel symbol rate, respectively. $P^{s,i}_{\text{rx}}$ is the received power at the end of span s. SNR_{TRx}, σ_{Flt}, σ_{Ag} are the transceiver SNR, SNR penalty due to wavelength selective switches filtering, and SNR margin due to the aging. Hence, the GSNR for all potential connections from arbitrary sources to destinations in the network can be computed. Subsequently, the modulation format profiles of the K shortest (path, channel, core)-tuples are pre-calculated, employing GSNR thresholds for each modulation format level [23]. To calculate the power of ICXTs due to the coupling of adjacent cores for MCF, we can apply $P^{s,i}_{\text{ICXT}} = \mu^{s,i}_{\text{ICXT}} P^{s+1,i}_{\text{tx}}$.

A MBoSDM does not need the MIMO DSP equipped transceivers when the accumulated ICXT penalty on the SNR is equal or lower than 1 dB [27]. The ICXT threshold of each modulation format level in terms of acceptable bit error rate (BER) according to the corresponding GSNR in dB based on (9) is as follows [20].

$$\mu^{m}_{\text{ICXT}_{\text{th}}} = 10\log_{10}\left(\frac{1-10^{\left(\frac{-\Gamma}{10}\right)}}{\chi^{m}\times 10^{\left(\frac{G_{\text{th}}}{10}\right)}}\right), \tag{9}$$

where $\mu^{m}_{\text{ICXT}_{\text{th}}}$ is the threshold of acceptable ICXT of modulation format level m for a given QoT penalty Γ and BER. Additionally, $\chi^{m=1}$ to $\chi^{m=6}$ equal 0.5, 1, 3.41, 5, 10, 21.

III. Proposed Algorithm

In this section, we introduce the proposed channel-based ICXT- and NLI-aware resource allocation algorithms specifically designed for the SD-EON controller. Utilizing the physical layer model described in Section II, the GSNR, supported modulation formats, and bandwidth for all channels along the K-shortest paths (KSPs) of all source-destination pairs are pre-calculated for both MCFs and BuMFPs in MB-EONs, enabling agile and efficient resource allocation. Building on this framework, we proposed two channel-based resource allocation methods for MCFs and compared their performance under dynamic scenarios with each other and with BuMFPs:

(I) **Core-Spectrum-Band (CSB)**: This method prioritizes the allocation of core resources over bands. All available bands within a single core are fully utilized before transitioning to the next core.

(II) **Band-Spectrum-Core (BSC)**: This method prioritizes the allocation of bands over cores. Channels within the C-band are allocated sequentially across all cores. Once the C-band resources are fully utilized, the allocation moves to the L-band on the first core and continues sequentially across cores and other available bands until all resources are exhausted.

It's important to note that in channel-based BuMFPs (CB-BuMFPs) approach, the First-Fit algorithm is used for core, band, and spectrum allocation, with bands considered in the order of C, L, and S.

To evaluate the performance of these resource allocation methods, we developed the ICXT- and NLI-Aware sliceable routing, modulation, core, band, and spectrum allocation (XT-NLI-A-RSA) algorithm (Algorithm 1). This algorithm incorporates pre-calculated physical layer parameters, including GSNR and supported modulation formats and bandwidth, to ensure that QoT requirements are met. The XT-NLI-A-RSA algorithm operates in two main stages. In the first stage, the algorithm attempts to serve the incoming request as a single chunk along the KSPs (Lines 2-9). For each path, the available channel vector (ACV) is calculated using the specified spectrum allocation method (SAM), which prioritizes either cores or bands. The ACV consists of free channels on the path that satisfy the continuity constraint and can support at least the PM-BPSK modulation format based on pre-calculated information (Line 3). Using the First-Fit approach, the algorithm identifies the first channel in the ACV that meets the QoT requirements, ensuring the channel's GSNR and supported modulation format are sufficient for the requested bandwidth. If such a channel is found, the resources (path, core, band, and channel) are allocated to the request, and the process terminates successfully (Lines 4-7). If the request cannot be allocated as a whole, the algorithm transitions to the second stage, where it slices the requested bandwidth into multiple segments based on the supported bandwidth of available channels along a single path (Lines 10–29). In this stage, the algorithm employs the First-Fit approach to find a suitable channel in the ACV. For each segment, the ACV is recalculated to ensure that each selected channel supports

Algorithm 1 ICXT- and NLI-Aware Sliceable Routing, Modulation, Core, Band and Spectrum Allocation (XT-NLI-A-RSA)

Inputs: (1) $KSPs$: Set of K-shortest paths, (2) bw_r: Bandwidth of request r, (3) MF^{i}_{path}: Pre-calculated modulation for channel i on $path$, (4) SAM: Spectrum Allocation Method.

Parameters: (1) bw_{rem}: Remaining bandwidth during slicing, (2) bw^{i}_{path}: Supported bandwidth for channel i on $path$, (3) ACV: Available channel vector.

Output: Path and Allocated Resources

1: $Allocated \leftarrow$ **False**
2: **for** ($path$ in $KSPs$) **do**
3: Find the first available channel in ACV using the first-fit approach and SAM, and assign its index to i
4: **if** i is valid **and** MF^{i}_{path} meets bw_r **then**
5: Allocate $path$, core, band, and channel to request r
6: $Allocated \leftarrow$ **True**
7: **return** Allocated resources for request r
8: **end if**
9: **end for**
10: **if** $Allocated$ is **False then**
11: **for** ($path$ in $KSPs$) **do**
12: $bw_{\text{rem}} = bw_r$
13: **while** $bw_{\text{rem}} > 0$ **do**
14: Find the first available channel in ACV using SAM, and assign its index to i
15: **if** i is valid **then**
16: Calculate bw^{i}_{path} based on MF^{i}_{path}
17: Allocate $path$, core, band, and channel to request r
18: $bw_{\text{rem}} \leftarrow bw_{\text{rem}} - bw^{i}_{path}$
19: **if** $bw_{rem} \leq 0$ **then**
20: $Allocated \leftarrow$ **True**
21: **return** All resources allocated to segments of request r
22: **end if**
23: **else**
24: Release all allocated resources to request r
25: **break**
26: **end if**
27: **end while**
28: **end for**
29: **end if**
30: **if** $Allocated$ is **False then**
31: Request r is blocked.
32: **end if**

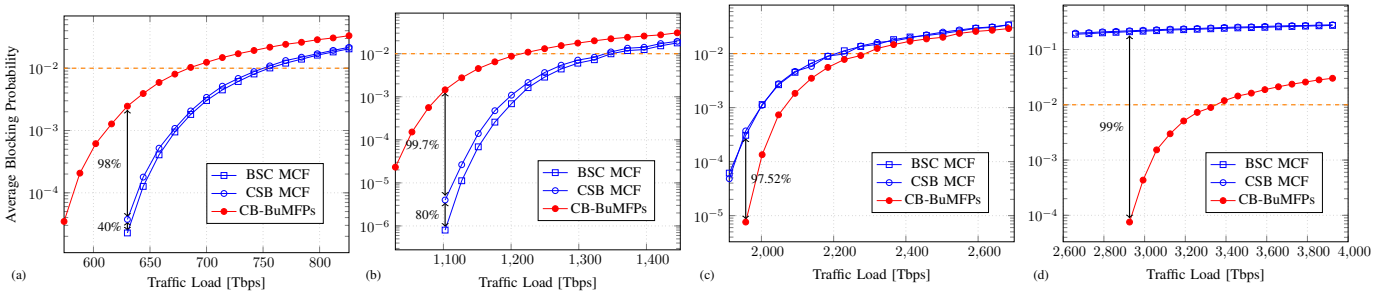

Fig. 1: Average request blocking probability for the US Backbone topology using BSC MCF, CSB MCF, and CB-BuMFPs approaches, for (a) 4, (b) 7, (c) 13, and (d) 19 cores/fibers.

at least the minimum required modulation format. Resources for each segment are allocated iteratively until either the entire request is fulfilled (Lines 14–22) or the available resources are exhausted. If allocation fails at any stage for a specific path, all previously assigned resources are released (Lines 23–26), and the algorithm attempts to allocate the request along the next path in the path set. Finally, if the request cannot be served through either full allocation or slicing, it is blocked (Lines 30–32).

IV. Simulation Results

In this section, we evaluate the performance of the proposed algorithm under various network configurations for the US Backbone topology using Fusion, an open-source Python-based SD-EON controller [28]. In this work, we consider KSPs with $K = 3$, where the minimum, maximum, and average path lengths, computed across all paths in the network, are 315.3 km, 6058.4 km, and 3174.4 km, respectively. In the simulation we consider the C, L, and S bands across different BuMFP and MCF configurations. BuMFPs consist of bundles containing 4, 7, 13, or 19 single-core fibers, while MCFs include fibers with 4, 7, 13, or 19 cores. In this paper, the core counts of 4, 7, 13, and 19 in MCFs are selected to balance capacity, ICXT, and manufacturability while ensuring practical feasibility. All configurations feature 80, 80, and 108 fixed-grid channels in the C, L, and S bands, respectively, each with a bandwidth of 75 GHz.

Request inter-arrival and holding times follow an exponential distribution, while requested bandwidths are uniformly distributed within the range of 100–600 Gbps, in increments of 100 Gbps. LCIs in the simulation support data rates ranging from 100 Gbps to 600 Gbps, corresponding to modulation formats from PM-BPSK to PM-64QAM. The average blocking probabilities are calculated to satisfy either a 95% confidence interval or a maximum of 50 independent iterations (seeds), with 15,000, 25,000, 50,000, and 75,000 requests per iteration for networks with 4, 7, 13, and 19 cores or fibers, respectively. The algorithm was tested under varying request volumes per seed, demonstrating that the network reached a steady state at the specified number of requests per trial.

Fig. 1 illustrates the blocking probability as a function of traffic load (in Tbps) for different configurations: MCF with CSB (CSB MCF), and BSC (BSC MCF) spectrum allocation methods, along with CB-BuMFPs. The subfigures (Fig. 1a, 1b, 1c, and 1d) present results for MCFs and BuMFPs with 4, 7, 13, and 19 cores/fibers, respectively, on the US Backbone topology. Fig. 2 and 3 illustrate the percentage of usage for each modulation format level and the average lightpath length in network configurations with 4, 7, 13, and 19 cores (or fibers). These configurations correspond to total traffic loads of 740, 1300, 2410, and 3520 Tbps, respectively, with each core handling 530 Erlangs of traffic.

On average, across all traffic loads, both MCF approaches reduce the blocking probability by more than 67% compared to CB-BuMFPs (Fig. 1a). The higher blocking probability of CB-BuMFPs stems from their higher loss coefficients, which limit the GSNR and restrict the use of higher modulation formats, resulting in fewer feasible lightpaths. In contrast, MCFs benefit from ultra-low ICXT and loss characteristics, enabling higher GSNR and modulation formats, resulting in lower blocking probabilities even at high traffic loads.

For MCFs with 4 cores, the modulation formats and GSNR vary significantly across bands due to differences in loss coefficients and ICXT. The C-band consistently supports higher modulation formats and GSNR compared to the L- and S-bands, as its lower loss and reduced ISRS effects contribute to better signal quality and higher transmission rates. The L-band generally outperforms the S-band by supporting higher modulation formats and GSNR due to its lower ICXT compared to the other bands. As a result, the BSC MCF approach reduces the blocking probability by around 40% at 630 Tbps traffic load and by approximately 10% on average across all traffic loads compared to the CSB MCF approach.

Fig. 2a illustrates the modulation format usage percentage for established demands approximately 740 Tbps traffic for MCF with $C = 4$, supporting the previously discussed points. Using MCFs enables the adoption of higher-level modulation formats compared to BuMFPs across all bands. Building on this discussion, the average lightpath length for MCFs is consistently higher than that of BuMFPs for all modulation formats except PM-64QAM, as shown in Fig. 3a. However, for PM-BPSK, the average lightpath length of BuMFPs is slightly higher due to their increased reliance on PM-BPSK during the RSA process. Fig. 2a shows that the CSB approach employs higher modulation levels compared to BSC. However, as illustrated in Fig. 3a, the average lightpath length in BSC is greater than in CSB. For instance, at PM-8QAM, the average

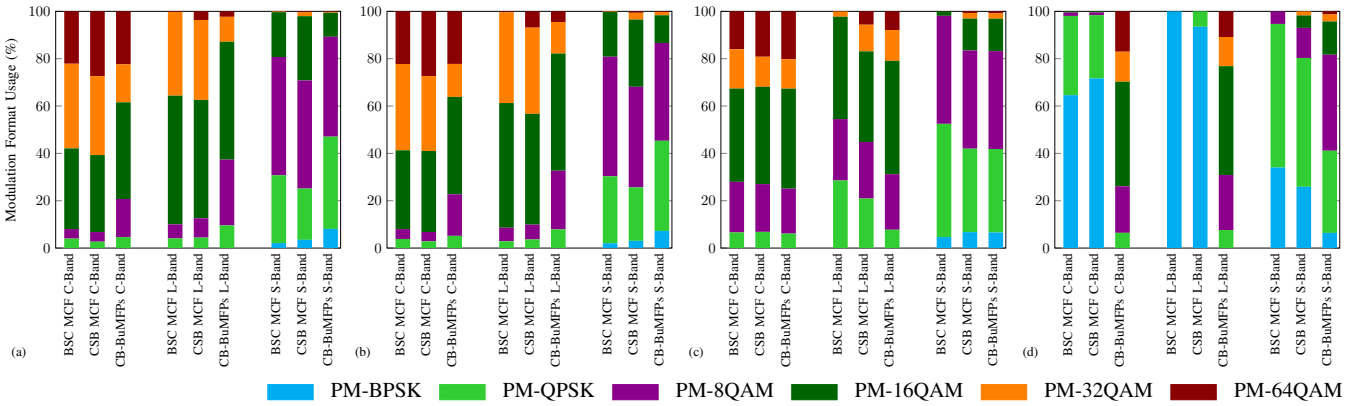

Fig. 2: Percentage usage of each modulation format level for established lightpaths in the US Backbone topology using MCF BSC, MCF CSB, and CB-BuMFPs approaches, categorized by band for (a) 4 (740 Tbps), (b) 7 (1300 Tbps), (c) 13 (2410 Tbps), and (d) 19 (3520 Tbps) cores/fibers based on the corresponding traffic load.

lightpath length in BSC is 15% longer than in CSB.

For $C = 7$, the larger core pitch of 51 µm significantly reduces ICXT compared to $C = 4$, improving GSNR and enabling the use of higher modulation formats across bands. This improvement is evident in Fig. 1b, where the blocking probability for MCF is significantly lower than that of BuMFPs at all traffic loads. Similar to $C = 4$, MCF consistently outperforms BuMFPs due to its lower loss coefficients. On average, across all traffic loads, both BSC and CSB MCF approaches reduce the blocking probability by more than 66% compared to CB-BuMFPs. The highest reductions are observed between 1,000 and 1,150 Tbps, where blocking is nearly eliminated.

The BSC MCF approach uses higher modulation formats for longer lightpaths, outperforming CSB MCF. It achieves an average blocking reduction of 20% across all traffic loads and a remarkable 80% reduction around 1,100 Tbps. Similar to $C = 4$, the CSB MCF approach at $C = 7$ employs higher modulation levels than BSC, as shown in Fig. 2b. However, Fig. 3b indicates that BSC MCF lightpaths with the same modulation format are longer, with PM-8QAM lightpaths in BSC averaging 19% longer than in CSB.

As the core count increases to 13 and 19, GSNR and modulation formats degrade due to reduced core pitch and thinner cladding, which result in higher ICXT and increased nonlinear noise. MCFs with $C = 13$ and especially $C = 19$ experience significant degradation, particularly in the C- and L-bands of $C = 19$, where many channels become unusable. Consequently, BuMFP outperforms MCF in terms of GSNR and modulation format levels for 13 and 19 fibers. Building on this, the simulation results for $C = 13$, shown in Fig. 1c, indicate that the blocking probability of CB-BuMFPs outperforms the CSB and BSC MCF. On average, across traffic loads ranging from 1,800 to 2,700 Tbps, the blocking probability in the US Backbone network with CB-BuMFPs (13 fibers) is approximately 34% lower than that of both the BSC and CSB approaches in the MCF system with $C = 13$. Additionally, the blocking probabilities of both MCFs with the BSC and CSB approaches are nearly identical for $C = 13$ due to the limited GSNR and high ICXT across all cores.

Fig. 2c illustrates the proportion of modulation format usage across all bands for a 2410 Tbps traffic load, showing that 67.9% of established lightpaths with CB-BuMFPs in the L-band use PM-16QAM and higher modulation levels, compared to 55.2% for CSB MCF and 45.5% for BSC MCF. Additionally, Fig. 3c shows that the average lightpath length for PM-16QAM is longer in BuMFPs than in BSC and CSB for $C = 13$, indicating that PM-16QAM is more frequently used in BuMFPs and supports longer connections compared to the other approaches.

As previously mentioned, MCF with $C = 19$ experiences a higher number of unusable channels due to elevated ICXT, resulting in a blocking probability exceeding 10% across all traffic loads for both BSC and CSB approaches, as illustrated in Fig. 1d. In contrast, blocking for CB-BuMFPs begins at approximately 3,000 Tbps traffic load, and on average, the blocking probability across loads ranging from 2,600 to 4,000 Tbps is reduced by 95% compared to both MCF approaches. Fig. 2d shows that, with MCF, at least 60% of the successful demands in the C- and L-bands utilize PM-BPSK modulation. However, in the S-band, the lower ICXT compared to the other bands results in increased utilization of PM-QPSK and PM-8QAM. Despite this improvement, the use of higher modulation formats in the S-band remains lower in MCFs compared to BuMFPs.

As shown in Fig. 3d, the increase in ICXT results in a reduced optical reach for all modulation formats compared to CB-BuMFPs. For instance, with PM-BPSK, the established connections in MCFs are at least 50% shorter than those in BuMFPs. Similarly, for PM-QPSK and PM-8QAM, the connection length is reduced by at least 45%. The differences become even more pronounced for higher-level modulation formats, with PM-16QAM showing the largest disparity—connection lengths in MCFs are over 70% shorter compared to BuMFPs. For PM-32QAM, the BSC approach is unable to utilize this modulation format entirely, and neither the BSC nor CSB approaches have used PM-64QAM for any connections.

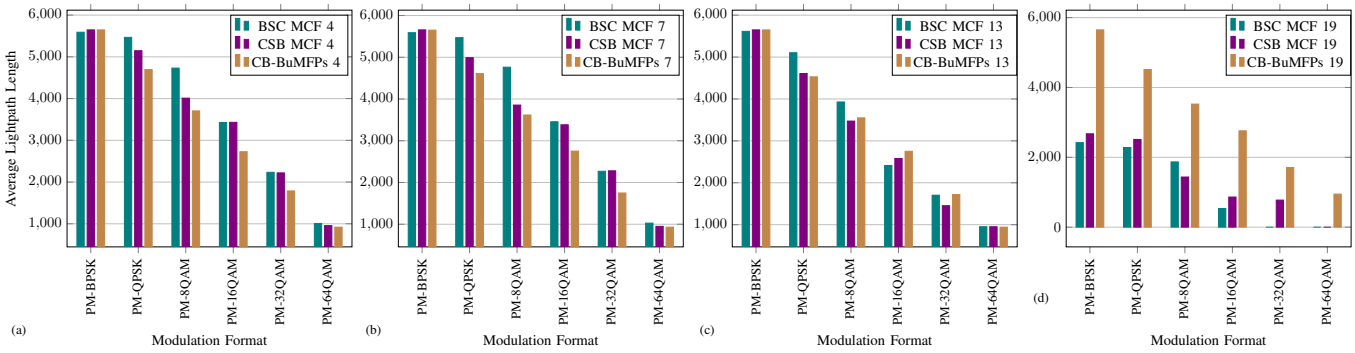

Fig. 3: Average established lightpath length in the US Backbone topology using MCF BSC, MCF CSB, and CB-BuMFPs approaches, categorized by modulation format level for (a) 4 (740 Tbps), (b) 7 (1300 Tbps), (c) 13 (2410 Tbps), and (d) 19 (3520 Tbps) cores/fibers, based on the corresponding traffic load.

V. Conclusion

This research has demonstrated the feasibility and effectiveness of a channel-based resource allocation approach for MBoSDM and multi-band BuMFPs optical networks, while explicitly accounting for the complex interplay of ICXT, ISRS, and NLIs. Our advanced GSNR model, combined with the innovative CSB and BSC algorithms, offers a robust and efficient solution to this challenging optimization problem. Comprehensive simulations on the US Backbone network validate our findings, demonstrating that the BSC MCF approach outperforms the CSB MCF and CB-BuMFPs approaches by reducing the blocking probability by approximately 40% and 99%, respectively, at a 630 Tbps traffic load with 4-core/fiber configurations. This work lays a strong foundation for future research into adaptive resource allocation and dynamic network optimization for next-generation optical networks.

References

[1] CISCO, "Pioneering the IP and Optical Transformation," 2024.

[2] F. Arpanaei *et al.*, "Physical-layer aware routing, modulation level and resource allocation of SDM networks over FM-MCFs," in *European Conference on Optical Communication (ECOC)*, 2019, pp. 1–4.

[3] T. Hoshida *et al.*, "Ultrawideband systems and networks: Beyond C+ L-band," *Proceedings of the IEEE*, vol. 110, no. 11, pp. 1725–1741, 2022.

[4] T. Matsui *et al.*, "Design and applicability of multi-core fibers with standard cladding diameter," *Journal of Lightwave Technology*, vol. 38, no. 21, pp. 6065–6070, 2020.

[5] P. J. Winzer *et al.*, "Fiber-optic transmission and networking: the previous 20 and the next 20 years," *Optics express*, vol. 26, no. 18, pp. 24 190–24 239, 2018.

[6] F. Arpanaei *et al.*, "QoT-aware performance evaluation of spectrally–spatially flexible optical networks over FM-MCFs," *J. of Optical Communications and Networking*, vol. 12, no. 8, pp. 288–300, 2020.

[7] R. S. Luís *et al.*, "Crosstalk impact on the performance of wideband multicore-fiber transmission systems," *IEEE Journal of Selected Topics in Quantum Electronics*, vol. 26, no. 4, pp. 1–9, 2020.

[8] J. L. Ravipudi *et al.*, "Does considering only crosstalk suffice for QoT-aware provisioning in multicore fiber networks?" in *2024 International Conference on Optical Network Design and Modeling (ONDM)*. IEEE, 2024, pp. 1–4.

[9] M. Klinkowski *et al.*, "Dynamic crosstalk-aware lightpath provisioning in spectrally–spatially flexible optical networks," *Journal of Optical Communications and Networking*, vol. 11, no. 5, pp. 213–225, 2019.

[10] S. Petale *et al.*, "TRA: an efficient dynamic resource assignment algorithm for MCF-based SS-FONs," *Journal of Optical Communications and Networking*, vol. 14, no. 7, pp. 511–523, 2022.

[11] J. L. Ravipudi *et al.*, "Impairment- and fragmentation-aware, energy-efficient dynamic RMSCA for SDM-EONs," *Journal of Optical Communications and Networking*, vol. 15, no. 9, pp. D10–D22, 2023.

[12] S. Petale *et al.*, "Machine learning aided optimization for balanced resource allocations in SDM-EONs," *Journal of Optical Communications and Networking*, vol. 15, no. 5, pp. B11–B22, 2023.

[13] A. Rezaee *et al.*, "Dynamic Crosstalk-Aware Routing, Modulation, Core, and Spectrum Allocation for Sliceable Demands in SDM-EONs," in *2024 IEEE 30th International Symposium on Local and Metropolitan Area Networks (LANMAN)*, 2024, pp. 76–81.

[14] N. Sambo *et al.*, "Provisioning in multi-band optical networks," *Journal of Lightwave Technology*, vol. 38, no. 9, pp. 2598–2605, 2020.

[15] E. Etezadi *et al.*, "Joint Fragmentation- and QoT-Aware RBMSA in Dynamic Multi-Band Elastic Optical Networks," in *2024 24th International Conference on Transparent Optical Networks*, 2024, pp. 1–5.

[16] J. L. Ravipudi *et al.*, "Impairment-and fragmentation-aware dynamic routing, modulation and spectrum allocation in C+ L band elastic optical networks using Q-learning," *Optical Switching and Networking*, vol. 47, p. 100717, 2023.

[17] F. Calderón *et al.*, "Heuristic approaches for dynamic provisioning in multi-band elastic optical networks," *IEEE Communications Letters*, vol. 26, no. 2, pp. 379–383, 2021.

[18] ——, "Dynamic resource allocation in different ultrawideband optical network topologies," in *2022 IEEE Photonics Society Summer Topicals Meeting Series (SUM)*. IEEE, 2022, pp. 1–2.

[19] Z. Luo *et al.*, "Survivable routing, spectrum, core and band assignment in multi-band space division multiplexing elastic optical networks," *Journal of Lightwave Technology*, vol. 40, no. 11, pp. 3442–3455, 2022.

[20] F. Arpanaei *et al.*, "Ultra-high-capacity band and space division multiplexing backbone EONs: multi-core versus multi-fiber," *J. of Optical Communications and Networking*, vol. 16, no. 12, pp. H66–H78, 2024.

[21] ——, "Analyzing Ultra-Low Inter-Core Crosstalk Fibers in Band and Space Division Multiplexing EONs," in *2024 15th International Conference on Network of the Future (NoF)*, 2024, pp. 164–168.

[22] R. McCann *et al.*, "FUSION: A Flexible Unified Simulator for Intelligent Optical Networking," in *IEEE International Conference on Advanced Networks and Telecommunications Systems (ANTS)*, 2024.

[23] G. Bosco, "Advanced Modulation Techniques for Flexible Optical Transceivers: The Rate/Reach Tradeoff," *Journal of Lightwave Technology*, vol. 37, no. 1, pp. 36–49, 2019.

[24] F. Ye *et al.*, "Simple analytical expression for crosstalk estimation in homogeneous trench-assisted multi-core fibers," *Opt. Express*, vol. 22, no. 19, pp. 23 007–23 018, Sep 2014.

[25] M. R. Zefreh *et al.*, "A Real-Time Closed-Form Model for Nonlinearity Modeling in Ultra-Wide-Band Optical Fiber Links Accounting for Inter-channel Stimulated Raman Scattering and Co-Propagating Raman Amplification," *2020, arXiv:2006.03088,[eess.SP]*.

[26] P. Poggiolini *et al.*, "Closed Form Expressions of the Nonlinear Interference for UWB Systems," in *European Conference on Optical Communication (ECOC)*, 2022, pp. 1–4.

[27] P. J. Winzer *et al.*, "Penalties from in-band crosstalk for advanced optical modulation formats," in *ECOC*, 2011, pp. 1–3.

[28] A. Rezaee *et al.*, "FUSION," https://github.com/SDNNetSim/FUSION, 2024.